Acta Geotechnica
https://doi.org/10.1007/s11440-024-02341-9

RESEARCH PAPER

Temperature effects on adsorption and capillarity water retention mechanisms in constrained unsaturated soils

Yu Lu[1] · John S. McCartney[1]

Received: 25 July 2023 / Accepted: 1 April 2024

Abstract
This paper focuses on the impact of elevated temperatures on the adsorptive and capillarity water retention mechanisms of unsaturated soils under constrained (constant volume) conditions. This topic is critical for simulating the thermo-hydraulic behavior of soils in hydrogeological or geotechnical applications, including climate change effects on near surface soils, energy piles or soil borehole thermal energy storage systems in unsaturated soil layers, and buffers for geological nuclear waste repositories. A nonisothermal soil water retention curve (SWRC) that separately considers the temperature-dependency of the key parameters governing adsorptive and capillarity water retention mechanisms and soil physical parameters (e.g., surface tension, contact angle, adsorption capacity, cation exchange capacity, mean cavitation suction, air entry value and equilibrium film thickness) was developed to provide insights into the impact of temperature on water retention over the full suction range. The nonisothermal SWRC was validated using experimental data on high plasticity clays, with a good prediction of temperature effects on adsorption and capillarity water retention mechanisms in constrained unsaturated soils.

Keywords Adsorption · Capillarity · Soil water retention · Temperature · Unsaturated soil

1 Introduction

The soil water retention curve (SWRC) is a fundamental constitutive relationship governing water storage in unsaturated soils that is used in quantifying water distribution and flow [16, 46]. The SWRC is also critical for interpreting the mechanical behavior of unsaturated soils, such as shear strength [18, 47], deformation [35, 48, 67], and effective stress [47, 114]. The SWRC reflects the equilibrium condition between the volumetric water content (or degree of saturation) and suction. Suction is composed of osmotic suction and matric suction components. Osmotic suction arises in the presence of chemical concentration gradients [84, 85], while matric suction describes the soil water potential with respect to pure water relative to ambient pore air pressure in the absence of a salt solution [16, 46]. The matric suction can be quantified by two physical mechanisms: (1) capillarity associated with the presence of a curved air-water meniscus between soil particles, and (2) adsorption associated with water retention on or within soil particles due exchangeable cation hydration, mineral surface hydration, or crystal interlayer surface hydration [46, 113]. The adsorption and capillarity mechanisms control the amounts of water storage in the hydration, pendular, funicular, and capillary regimes of the SWRC when moving from high to low matric suction values [12].

Because the SWRC governs the interactions between soil particles, pore air, and pore water, there are a number of variables that affect the SWRC, including those related to particle mineralogy variables (e.g., cation exchange capacity, specific surface area, etc.), soil structure variables (e.g., void ratio, pore size distribution, etc.), and environmental variables (e.g., temperature, humidity, etc.) and pore fluid characteristics (e.g., pH, salinity, etc.) [3, 11, 19, 20, 36, 37, 39, 43, 65, 84, 89, 115]. Multiple

✉ John S. McCartney
mccartney@ucsd.edu

Yu Lu
yu-lu@ucsd.edu

[1] Department of Structural Engineering, University of California San Diego, 9500 Gilman Dr., La Jolla, CA 92093-0085, USA

Published online: 20 May 2024

parameterized SWRC models have been proposed to represent the evolution of the SWRC over the full suction range, while temperature effects have seldom been considered from a mechanistic perspective.

Given the emergence of hydrologic problems associated with nonisothermal near-surface water flow in soils associated with climate change and geotechnical problems that involve nonisothermal analysis (such as thermally active geotechnical structures combined with geothermal heating/cooling systems, and radioactive waste geological disposal repositories), there is an urgent need to investigate the SWRC under elevated temperatures. Several researchers have performed experimental tests to examine changes in the shape of the SWRC at high temperatures and generally revealed a downward shift of the SWRC, resulting in a decrease in volumetric water content under constant suction [22, 25, 57, 63, 89, 91, 95, 99, 100]. This phenomenon is typically explained by temperature-induced changes in soil and water physicochemical parameters (e.g., surface tension, contact angle, clay fabric, pore water chemistry, etc.) [4, 15, 69, 72, 99]. Several temperature-dependent variations have been incorporated into the existing SWRC models originally developed for isothermal conditions [6, 25, 33, 41, 63, 70, 76, 78, 80, 86, 118]. For instance, Grant and Salehzadeh [25] explored temperature effects on the water-air interfacial tension, contact angle, and the enthalpy of immersion per unit area. They proposed an equation describing the matric suction between the elevated and reference temperatures. A similar approach was adopted in other studies [2, 4, 78]. Some researchers have extended the water retention regimes-based SWRC model into nonisothermal conditions. For example, Vahedifard et al. [87] analyzed the temperature effects on adsorption and capillarity water retention mechanisms separately and found that temperature effects on the SWRC of sands, silts, and clay can be significant, particularly for fine-grained soils subjected to high temperatures (e.g., > 60 °C). Recently, McCartney [60] proposed a conceptual model based on the Lu [46] SWRC model considering temperature effects on surface tension, wetting fluid-solid contact angle, cavitation suction, maximum adsorption capacity, and maximum suction to characterize the coupled thermo-hydraulic properties of MX80 bentonite in engineered barrier systems. The conceptual model indicated that water retention may increase or decrease with temperature in different water retention regimes due to the temperature dependency of these different parameters. However, the specific relationships between the aforementioned parameters and temperature, as well as their underlying mechanisms, were not fully explored.

Understanding temperature effects on the SWRC across the full matric suction range is particularly important for compacted sodium bentonite used as a buffer material in high-level radioactive waste (HLW) disposal repositories [14, 54–56, 64, 77, 107, 116, 119]. This is especially the case as the temperatures in buffer systems in repositories may reach values up to 200 °C, much higher than that in other hydrologic systems or geotechnical applications [26, 52, 53, 117]. Lu and McCartney [51, 52] conducted tank-scale tests on compacted MX80 bentonite and measured temperature-dependent transient SWRCs at different locations under coupled heat transfer and water imbibition processes with a central temperature of 200 °C simulating high thermal gradients in the repository. Sanchez [73], Lloret and Villar [44] proposed an empirical equation for the SWRC of compacted FEBEX bentonite. With the experimental SWRCs of compacted MX80 bentonite determined under controlled temperatures, Jacinto et al. [33] modified the SWRC model of van Genuchten [88] by considering the temperature effects on porosity, air entry suction, slope coefficient of the linear part of the retention curve, as well as the saturated water content. Wan et al. [99] investigated the temperature effects on the SWRC of compacted GMZ01 bentonite at temperatures ranging from 20 to 80 °C and reported that the influence of temperature on the water retention capacity significantly depends on suction. However, the concept of residual water content (or residual suction) may be an artifact of the way that the SWRC has been measured in the past (e.g., liquid outflow using a pressure plate) and that if vapor equilibrium had been used, they might have been able to reach a maximum suction. Modifying the SWRC of Lu [46] provides a more fundamental approach to considering the different ways that temperature may affect water retention over the full range of suction.

In this study, a new nonisothermal SWRC that separately considers the temperature-dependency of the key parameters governing different water retention mechanisms and soil physical parameters was developed to provide insights into the impact of temperature on water retention over the full suction range. The new nonisothermal SWRC model will be useful for simulating coupled heat transfer and water flow processes in hydrogeologic and geotechnical applications involving elevated temperatures.

2 Background

Among the isothermal SWRC models, three widely used SWRC models are those of Brooks and Corey [8], van Genuchten [88], and Fredlund and Xing [17]. These SWRC models have parameters that describe the shape of the SWRC in the capillary regime established from experimental studies (i.e., a parameter describing the air entry suction and a parameter describing the pore size

distribution) but do not clearly distinguish between the different water retention mechanisms beyond a parameter governing the residual degree of saturation. Building on the model of Revil and Lu [66], Lu [46] proposed a generalized SWRC that more explicitly considers the adsorption and capillarity water retention mechanisms by introducing four new matric suction-related parameters (i.e., adsorption capacity, adsorption strength, mean cavitation, and maximum suction), as described by the following set of equations:

$$\theta(\psi) = \theta_{\mathrm{a}}(\psi) + \theta_{\mathrm{c}}(\psi) \tag{1}$$

$$\theta_{\mathrm{a}}(\psi) = \theta_{\mathrm{a,max}}\left\{1 - \left[\exp\left(\frac{\psi - \psi_{\max}}{\psi}\right)\right]^{M_{\mathrm{L}}}\right\} \tag{2}$$

$$\theta_{\mathrm{c}}(\psi) = \frac{1}{2}\left[1 - \mathrm{erf}\left(\sqrt{2}\frac{\psi - \psi_{\mathrm{c}}}{\psi_{\mathrm{c}}}\right)\right] [\theta_{\mathrm{s}} - \theta_{\mathrm{a}}(\psi)]\left[1 + (\alpha\psi)^{N_{\mathrm{L}}}\right]^{1/N_{\mathrm{L}}-1} \tag{3}$$

where ψ is the matric suction (kPa), $\psi_{\max}$ is the maximum matric suction (kPa) which corresponding to the endpoint of the SWRC when the water content is zero, ψ_{c} is the mean cavitation suction (kPa) that is associated with the physical-phase transition point between the adsorption and capillarity mechanisms, $\theta(\psi)$ is the (volumetric) water content (m^3/m^3) corresponds to the suction ψ, $\theta_{\mathrm{a}}(\psi)$ and $\theta_{\mathrm{c}}(\psi)$ represent the water content (m^3/m^3) corresponds to the adsorption and capillarity mechanism respectively, θ_{s} is saturated water content (m^3/m^3) equal to porosity of the soil, $\theta_{\mathrm{a,max}}$ is the adsorption capacity (m^3/m^3) which corresponds to the maximum water content contributed by the adsorption mechanism, M_{L} is the adsorption strength (dimensionless) that controls the changing rate of adsorption near the maximum matric suction and is only controlled by mineral type and quantity and bears little relation to pore-size distribution, N_{L} is capillary pore-size distribution parameter (dimensionless) that controls the curve slope in the capillary regime, α is the reciprocal of the air entry suction (1/kPa) which is associated with the inflection point of the SWRC at high water content range, and erf() is the error function. An essential feature of Eq. (2) is that the parameter M_{L} does not control the total amount of the adsorbed water, which is governed by the adsorption capacity $\theta_{\mathrm{a,max}}$. Cavitation is the process of forming vapor bubbles inside or on the boundary of a liquid body under tension. This phase transition phenomenon generally occurs in water when the liquid water pressure falls below the saturated vapor pressure, in which case the intermolecular water pressure essentially reaches the tensile strength of liquid water [7, 58]. Although the parameter ψ_{c} in Eq. (3) has a clear physical meaning, the method to determine this parameter is not well established, meaning that the value of ψ_{c} is essentially used as a fitting parameter in practice. While the SWRC model of Lu [46] was developed for isothermal conditions, the fact that it explicitly considers the adsorption and capillarity water retention mechanisms facilities the incorporation of temperature effects into the individual parameters. Similar to Lu [46], the term "suction" in follow context refers specifically to matric suction, excluding osmotic effects.

3 Nonisothermal SWRC model

The proposed nonisothermal SWRC model is developed based the individual ways that temperature may affect the adsorption and capillarity water retention mechanisms. In a water-saturated soil, there are three types of pore water, including bound water, capillary water that can be drained, and trapped water that is not bound or drainable. Among them, the sum of the bound water plus the trapped water is attributed to the adsorption force [66]. Without loss of generality of the water retention mechanism, this study mainly focuses on the high plasticity clayey soils used in nuclear waste repository buffer systems (e.g., Boom clay, bentonite, etc.), which show significant adsorption compared to granular soils and retain water over a wide range of suction. Although bentonite is composed of various minerals, the main constituent is montmorillonite (above 75–95%), which controls the soil water retention characteristics and other performance features of buffer systems [44, 91, 92, 99]. The influence of other minor mineral components in bentonite (i.e., quartz, plagioclase, calcite, etc.) is not in the scope of this paper. It is useful to first review the effects of temperature on each of the key parameters in the SWRC of Lu [46] focusing on a monodispersed bentonite with particle-scale characteristics represented by those of montmorillonite. This assumption is necessary to effectively up-scale from the particle scale to the soil macrostructure scale in evaluating temperature effects. Although the SWRC can be expressed as a relation between suction and gravimetric water content [99, 112], the SWRC form of Lu [46] and some other works [60, 66, 71, 87], i.e., suction vs. volumetric water content or degree of saturation is used in this study. This approach simplifies issues in converting between gravimetric and volumetric water contents due to the greater density of adsorbed pore water.

3.1 Temperature effects on adsorption

Adsorption occurs at high suctions or low water contents, where cation hydration, crystal layer surface hydration, and particle surface hydration take place [38, 61]. Cation hydration operates in the maximum matric suction range as its origin is the Coulomb electric force at the atomic scale.

Although an approximately constant value of the maximum matric suction (e.g., ~ 1.0 GPa) was assumed in some previous studies on the SWRC [17, 46, 99], it should be noted that this parameter is intrinsically related to the endpoint of the SWRC when the soil is dry, while the value could be temperature dependent. Lu and Khorshidi [49] proposed a relationship for the maximum suction based on the Brunauer-Emmett-Teller (BET) model [9], given as follows:

$$u_{\max} = \frac{RT}{3000 v_w} c \tag{4}$$

$$c = \exp\left(\frac{E_1 - E_L}{RT}\right) \tag{5}$$

where $u_{\max}$ is the maximum suction (kPa), v_w is the molar volume of water (0.000018 m^3/mol), R is the universal gas constant (8.31432 J/mol/K), T is the absolute temperature in Kelvin, c is the BET equilibrium constant of the soil (dimensionless) that related to the enthalpy of sorption for the first molecular layer of water (Fig. 1), E_1 is the heat of adsorption for the first layer, E_L is the heat of adsorption for the second and higher layers and is equal to the heat of liquefaction. The difference between the two energy parameters (E_1-E_L) in the exponent is the energy needed to transfer from adsorbed gas to liquid. Since the (E_1-E_L) is independent of temperature, the temperature-dependence of parameter c can be determined by Eq. (5). Here, the maximum suction $u_{\max}$ can be regarded as maximum matric suction $\psi_{\max}$ as the gravitational and osmotic contributions are assumed to be negligible. An example of the temperature dependence of $\psi_{\max}$ for temperatures between 273 to 473 K is shown in Fig. 1.

For suctions below $\psi_{\max}$, the van der Waals force is primarily responsible for inner-layer surface hydration, and particle surface hydration gradually plays a significant role

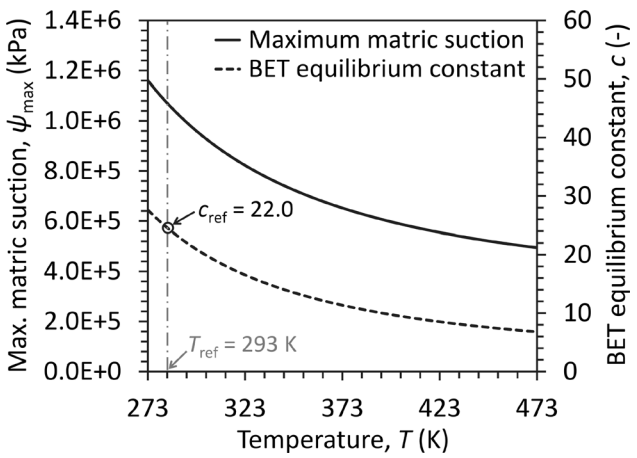

Fig. 1 Example of the temperature dependence of maximum matric suction and BET equilibrium constant of MX80 bentonite

as the Coulomb force diminishes rapidly as hydration water increases beyond a few layers of water molecules. The total amount of the adsorption water, controlled by both Coulomb and van der Waals forces, corresponds to the adsorption capacity near the lower bound suction of the adsorption [66, 83]. As previous definitions for the adsorption capacity have issues when applied to compacted soils [66], a new equation for the adsorption capacity is proposed:

$$\theta_{a,\max} = (1 - \theta_s)\left(\frac{CEC}{\overline{\xi}_s} + b_w\right) \tag{6}$$

where $\theta_{a,\max}$ is the adsorption capacity (m^3/m^3), CEC is the cation exchange capacity (meq/g), b_w is a temperature-dependent model parameter associated with the amount of water trapped in the pore space during desorption that denotes the excess mass of water per gram of dry soil, on the order of 0.10 g/g [66], and $\overline{\xi}_s$ is a model parameter reflecting the slope of the sorption curve that can be calculated as follows:

$$\overline{\xi}_s = \frac{c - 1}{c} \frac{CEC_r}{v_{m,r}} \tag{7}$$

where v_m represents the gravimetric water content when the first monolayer is fully saturated, CEC_r and $v_{m,r}$ are the values of CEC and v_m at a reference temperature of 293 K. For clay minerals with high CEC, the value of $\overline{\xi}_s$ is calculated to be 2.80 (with the same units as the CEC) [66]. In the second bracket in Eq. (6), the first term primarily is associated with the soil mineralogy, while the second term is associated with the pore structure and pore size distribution.

The temperature dependence of the CEC has been observed in the literature and has been used to explain the temperature effect on the swelling potential of expansive soils, as the CEC is related to the thickness of the double diffuse layer (DDL) [82, 109, 120]. For lower temperature ranges between 293 and 373 K, a small increase in the CEC has been observed by some researchers [24, 97]. An increasing trend of swelling pressure with temperature rises from 293 to 363 K has been reported on sodium bentonite, while the changing rate decreases with increasing temperature [1, 5, 108]. Furthermore, after a threshold, the swelling potential may have a decreasing trend. In fact, the decrease in CEC with increasing temperature under high-temperature conditions (e.g., above 373 K) has been widely confirmed and can be interpreted from the point that the capacity of a soil particle holding exchangeable cations depends on the size of the double diffuse layer and the dipolar water that is attracted to that layer [62, 74, 120]. One hypothesis is that when extremely high temperatures are applied to a soil, the DDL thickness is diminished

because the heat removes the dipolar water from the DDL and carries with it exchangeable cations [24].

Thus, the reduction of the thickness of the DDL with temperature corresponds to a reduction in the *CEC* of soil. The temperature dependence of *CEC* can be expressed as follows:

$$CEC = \frac{1}{2} CEC_{\max} \left[\cos\left(A\pi \frac{BT - T_1}{T_2 - T_1} \right) + 1 \right] \tag{8}$$

where $CEC_{\max}$ is the maximum value of *CEC*, T_1 is the temperature corresponding to the $CEC_{\max}$ typically occurs around 373 K (100 °C), T_2 is the temperature corresponding to $CEC_{\min}$, which typically occurs around 1273 K (1000 °C), A and B are parameters which are typically close to unity. A fitting of Eq. (8) to data for different soils under various temperatures is shown in Fig. 2. Thus, the temperature dependence of adsorption capacity can be estimated by the change of *CEC* under various temperatures. Through the analysis above, an example of the temperature dependence of adsorption capacity (b_w is assumed as constant here) and *CEC* for MX80 bentonite with a dry density of 1.6 Mg/m^3 are shown in Fig. 3.

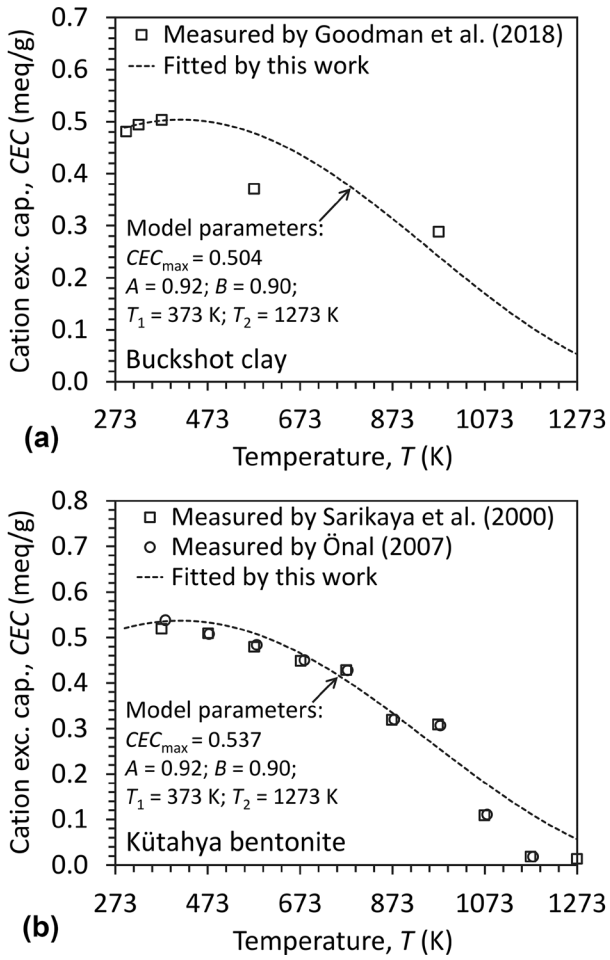

Fig. 2 Relationship between *CEC* and temperature: **a** Buckshot clay; **b** Kütahya bentonite

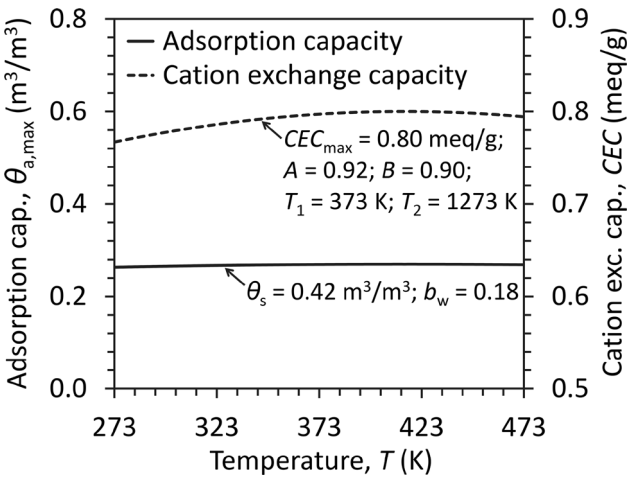

Fig. 3 Example of the temperature dependence of adsorption capacity and cation exchange capacity of MX80 bentonite with a dry density of 1.6 Mg/m^3

3.2 Temperature effects on capillarity

The temperature effects on capillarity water retention mechanisms have been well studied in the literature, with temperature affecting the interfacial surface tension, fluid-solid contact angle, and enthalpy of immersion [25, 78, 87]. The study in this work follows a similar approach to these studies but involves a new way to determine the mean cavitation suction and its temperature dependence. Matric suction arising from the capillarity water retention mechanism can be described by the Young-Laplace equation [110]:

$$\psi = \frac{2\sigma\cos\beta}{r} \tag{9}$$

where σ is the water-air interfacial tension (N/m), r is the pore size (the average radius of the water-air interface, in meters), β is the contact angle of the water-air interface with the solid (in radians). The term cos β is alternately known as the "wetting coefficient" [25].

The partial derivative of ψ with respect to temperature can be expressed as [4, 87]:

$$\frac{\partial\psi}{\partial T} = \frac{\psi}{\sigma}\frac{\partial\sigma}{\partial T} + \frac{\psi}{\sigma\cos\beta}\frac{\partial(\cos\beta)}{\partial T} \tag{10}$$

The temperature effect on water-air interfacial tension can be described by [27]:

$$\sigma = A_1 + B_1 \cdot T \tag{11}$$

where T is the absolute temperature in Kelvin, A_1 and B_1 are fitting parameters, suggested by Haar et al. [60] through

regression analysis as 0.11766 N/m and − 0.0001535 N/m/K, respectively.

Grant and Salehzadeh [25] demonstrated that incorporating a temperature-dependent contact angle allows the temperature derivative of the wetting coefficient, cos β, to be expressed in terms of independently measurable physical-chemical quantities as follows:

$$\frac{d\cos\beta}{dT} = \frac{1}{\sigma}\left(\frac{\sigma\cos\beta + \Delta h}{T} - \cos\beta\frac{d\sigma}{dT}\right) \tag{12}$$

where Δh is the enthalpy of immersion per unit area (J/m^2). The temperature dependence of enthalpy can be expressed as follows [87, 101]:

$$\Delta h = \Delta h_{\mathrm{r}}\left(\frac{1 - T_{\mathrm{r}}}{1 - T}\right)^{0.38} \tag{13}$$

where T_{r} is the reference temperature (K), Δh_{r} is the enthalpy of immersion per unit area at T_{r}, and − 0.516 J/m^2 is adopted for high plasticity clay in this work.

The solution of Eq. (12) enables the calculation of the wetting coefficient, cos β, as a function of temperature. By substituting Eq. (11) into Eq. (12), a general form can be obtained as follows:

$$\left(A_1 \cdot T + B_1 \cdot T^2\right)\frac{d\cos\beta}{dT} - A_1 \cdot \cos\beta = \Delta h \tag{14}$$

Solving Eq. (14) for cosβ yields the temperature-dependent form of the contact angle, given as follows:

$$\cos\beta = \frac{C_1 \cdot T - \Delta h}{A_1 + B_1 \cdot T} \tag{15}$$

where C is a constant (J/m^2/K) that can be determined as follows [25]:

$$C_1 = \frac{\Delta h_{\mathrm{r}} + A_1(\cos\beta)_{\mathrm{r}} + B_1(\cos\beta)_{\mathrm{r}} \cdot T_{\mathrm{r}}}{T_{\mathrm{r}}} \tag{16}$$

where $(\cos\beta)_{\mathrm{r}}$ is the wetting coefficient at reference temperature with a value close to 1.0. A value of − 0.00151 for parameter C_1 was calculated and utilized for high plasticity clays in this work. Using the definitions of Δh and C_1, Eq. (10) can be rewritten as follows:

$$\psi = (\chi + T)\frac{\partial\psi}{\partial T} \tag{17}$$

where χ is the temperature correction factor (K), determined as follows:

$$\chi = -\frac{\Delta h}{C_1} \tag{18}$$

By separation of variables and integration, Eq. (17) leads to the following closed-form expression for the nonisothermal matric suction in the capillary regime, as follows [25, 87]:

$$\psi = \psi_{\mathrm{r}}\left(\frac{\chi + T}{\chi_{\mathrm{r}} + T_{\mathrm{r}}}\right) \tag{19}$$

where ψ_{r} is the matric suction at a reference temperature (kPa).

Another important parameter related to capillarity in Eq. (3) is the mean cavitation suction represented by ψ_{c}. The mean cavitation suction is a threshold value between the capillarity and adsorption water retention mechanisms, and should be temperature-dependent. For soil under a matric suction near the mean cavitation suction, most of the pore water is assumed to be in the form of continuous films on the soil particle surfaces or liquid menisci lenses between particles. When wetting from this suction value, the soil particle surfaces become coated by thick water films and capillarity plays a dominant role. When drying from this suction value, the free water tends to cavitate and turns to vapor, and liquid water remains only in the form of adsorptive films bound onto or within the soil particles. A challenge is that Lu [46] did not provide guidance on how to determine this important parameter.

The mean cavitation suction is assumed to be related to the maximum adsorption water content because it also represents the boundary between the adsorption and capillarity water retention mechanisms. The gravimetric water content w (g/g) due to adsorption can be calculated using the specific surface area SSA (m^2/g), and the equilibrium film thickness H (m) as follows [83, 114]:

$$w = \rho_{w,\mathrm{ave}} \cdot SSA \cdot H \tag{20}$$

where $\rho_{w,\mathrm{ave}}$ is the average density of water film (g/m^3). The gravimetric water content can be converted to volumetric water content, as follows:

$$\theta = \frac{w \cdot \rho_{\mathrm{d}}}{\rho_{w,\mathrm{ave}}} = \rho_{\mathrm{d}} \cdot SSA \cdot H \tag{21}$$

where ρ_{d} is the dry density of the soil (g/m^3). Considering van der Waals forces as the governing component of adsorption on the soil particle surface, H can be expressed as a function of matric suction [32, 50]:

$$H = \left(\frac{A_H}{6\pi\psi}\right)^{1/3} \tag{22}$$

where A_H is the Hamaker constant that can be calculated by the Lifshitz theory [42] using the interaction of static dielectric constant in a medium [31, 79], as follows:

$$A_H = \frac{3}{4}k_{\mathrm{B}}T\left(\frac{\varepsilon_s - \varepsilon_w}{\varepsilon_s + \varepsilon_w}\right)^2 + \frac{3h_P v_e}{16\sqrt{2}}\frac{\left(RI_s^2 - RI_w^2\right)^2}{\left(RI_s^2 + RI_w^2\right)^{3/2}} \tag{23}$$

where k_{B} is the Boltzmann constant (1.3806505 × 10^{-23} J/K), h_P is the Planck constant (6.626068 × 10^{-34} Js), v_e is the main electronic adsorption frequency in ultraviolet

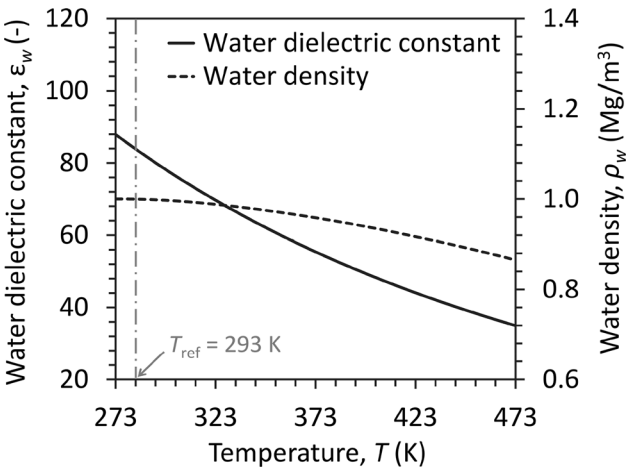

Fig. 4 Relationship between water dielectric constant, water density and temperature

light, ε_s is the dielectric constant of soil particle, ε_w is the dielectric constant of water (Fig. 4), RI_s is the refractive index of soil particle, RI_w is the refractive index of water. The effects of temperature on the dielectric properties of major soil constituents have been previously characterized. The impact of changing temperature on the dielectric constant of soil solids and air is negligible [102, 103]. Based on the work by Fernández et al. [13], Marshall [59] proposed an equation to describe the dielectric constant of water ε_w for water density ranging from 0.25 to 1.1 Mg/m^3 and temperature ranging from 238 to 1196 K, as follows:

$$\lg\left(\varepsilon_w - 1\right) = 0.7017 + \frac{642.0}{T} - \frac{1.167 \times 10^5}{T^2} + \frac{9.190 \times 10^6}{T^3} + \left(1.667 - \frac{11.41}{T} - \frac{3.526 \times 10^4}{T^2}\right)\lg \rho_w \tag{24}$$

where ρ_w is the density of water (Fig. 4). Although the refractive index varies with soil mineralogy and wavelength, the value of refractive index for most minerals is around 1.55, except for hematite and goethite, respectively [23]. For a given wavelength, the temperature dependence on the refractive index of water is mainly due to the change in water density. Note that the decrease in water refractive index from 273 to 373 K (with various wavelengths) is only about 1.2% [34, 75]. Thus, in this study, constant values of 1.55 and 1.33 were selected for the refractive index of soil and water in Eq. (16) for simplicity.

Since the intermolecular adsorptive forces elevate the water pressure locally, rendering adsorbed water less likely to cavitate than capillary water, the occurrence of cavitation can potentially be used to distinguish between the adsorption and capillarity water retention mechanisms and clarify the transitional behavior in soil water retention [58]. Moreover, a mean value of cavitation suction can be adopted for probabilistic analysis of the cavitation process, as cavitation is believed to be a rapid yet smooth process over a range of suctions that can be well described by a probability distribution function such as the normal distribution [29, 46]. Thus, by combining Eqs. (21) and (22) and replacing the matric suction ψ in Eq. (22) with the mean cavitation suction ψ_c and the volumetric water content θ in Eq. (21) with $\theta_{a,max}$, the mean cavitation suction ψ_c can be determined:

$$\psi_c = \frac{A_H}{6\pi}\left(\frac{\theta_{\mathrm{a,max}}}{\rho_{\mathrm{d}} \cdot SSA}\right)^{-3} \tag{25}$$

In Eq. (25), the value of ρ_{d} is assumed to be constant for the soil under constrained conditions. The *SSA* may vary with the temperature, but the change is expected to be small, especially for the temperature ranges representative of hydrological and geotechnical applications. Thus, a constant value of *SSA* is selected for simplifying fitting work in this study. The temperature effect on the $\theta_{\mathrm{a,max}}$ has been analyzed above (Fig. 2), while the temperature dependence of the ψ_c and A_{H} for MX80 bentonite with 1.6 Mg/m^3 in dry density is shown in Fig. 5. Curves in the figure show an increasing trend of ψ_c with increasing temperature, indicating that the suction range controlled by the adsorption mechanism becomes smaller. In other words, higher suction is required to follow the drying-path SWRC under elevated temperatures to reach the adsorption mechanism. Due to the negative correlation between temperature and maximum suction (Fig. 1), the positive correlations between temperature and adsorption capacity

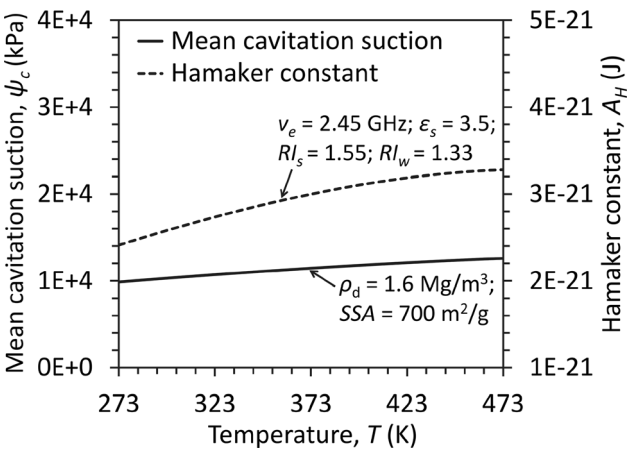

Fig. 5 Example of the temperature dependence of mean cavitation suction and Hamaker constant of MX80 bentonite with dry density of 1.6 Mg/m^3

(Fig. 3) and the positive correlation between temperature and mean cavitation suction (Fig. 5), the shape of the SWRC at low degrees of saturation becomes flatter with increasing temperature.

Experimental evidence reveals that the air entry suction ψ_{aev} decreases as temperature increases [10, 99]. Meanwhile, for suctions higher than ψ_{aev}, the SWRCs at different temperatures are almost parallel, suggesting that parameter n of the SWRCs are not significantly affected by temperature. Therefore, the SWRC model of Lu [46] can be extended to a new one that can takes into account temperature effects by only introducing the temperature influence on the ψ_{aev}. The relationship between the air entry suction and temperature can be described as follows:

$$\psi_{aev} = \exp\left[\eta\left(\frac{T_r}{T} - 1\right)\right]\psi_{aev,r} \tag{26}$$

where $\psi_{aev,r}$ is the air entry suction (kPa) at the reference temperature T_r, and η is a soil texture-related coefficient. The relationship between the air entry suction and temperature for Boom clay and GMZ01 bentonite is shown in Fig. 6. The magnitude of ψ_{aev} depends on the soil mineralogy and particle size distribution. For example, the value for GMZ01 bentonite (Fig. 6b) is greater than the value for Boom clay (Fig. 6a) at the same dry density.

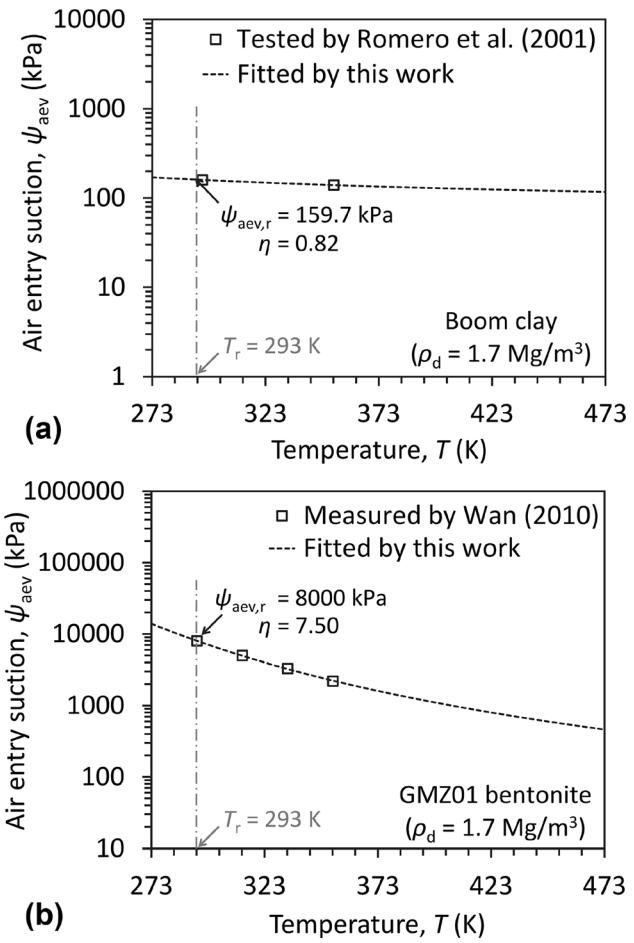

Fig. 6 Relationship between air entry suction and temperature: **a** Boom clay; **b** GMZ01 bentonite

In summary, the new nonisothermal SWRC based on the SWRC model of Lu [46] is defined using a set of three equations:

$$\theta(\psi, T) = \theta_a(\psi, T) + \theta_c(\psi, T) \tag{27}$$

$$\theta_a = \theta_{a,max}(T)\left\{1 - \left[\exp\left(\frac{\psi - \psi_{max}(T)}{\psi}\right)\right]^M\right\} \tag{28}$$

$$\theta_c = \frac{\theta_s - \theta_a}{2}\left\{1 - \mathrm{erf}\left[\sqrt{2}\frac{\psi}{\psi_c(T)}\left(\frac{\chi(T) + T}{\chi_r + T_r}\right) - \sqrt{2}\right]\right\} \cdot \left\{1 + \left[\alpha\psi\left(\frac{\chi(T) + T}{\chi_r + T_r}\right)\right]^N\right\}^{1/N-1} \tag{29}$$

In these equations, the temperature-dependent values of $\theta_{a,max}$, ψ_{max} (u_{max}), ψ_c and χ are defined using Eqs. (6), (4), (25), and (18). When incorporating the effects of temperature on the suction at elevated temperature in the capillary regime from Eq. (19), the r subscript is dropped from the suction at the reference temperature as the temperature-dependency arises from the parameters listed in the previous sentence. The temperature-dependency for α can be considered by the inverse of the ψ_{aev} defined by Eq. (26). The value of θ_s is assumed to be constant for constrained unsaturated soil. M is assumed to only be related to the clay mineralogy and is not considered to be temperature-dependent, while N is related to the pore size distribution and is also assumed to not be temperature-dependent for simplicity. A causal diagram for the parameters of the nonisothermal SWRC is depicted in Fig. 7. An example of the nonisothermal SWRC model for adsorption and capillarity regimes for MX80 bentonite with

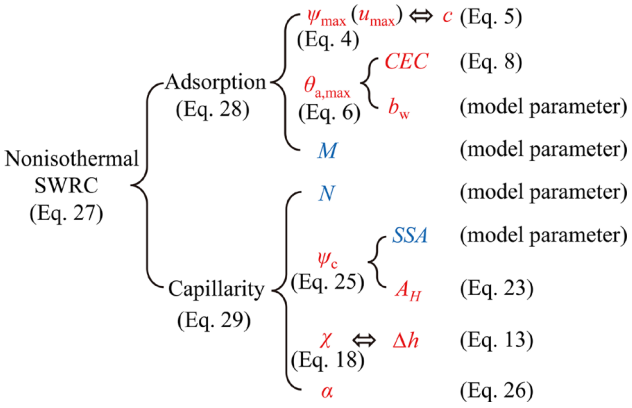

Fig. 7 Causal diagram of the parameters of the nonisothermal SWRC (nonisothermal parameters marked in red and isothermal parameters in blue)

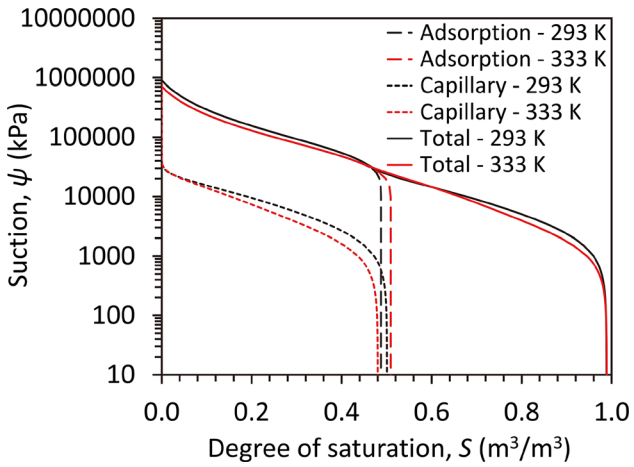

Fig. 8 Schematic diagram of nonisothermal SWRC considering the effects of temperature on the adsorption and capillarity water retention mechanisms

1.45 Mg/m^3 in dry density is shown in Fig. 8 for temperatures of 293 and 333 K.

4 Model validation

To validate the performance of the new proposed nonisothermal SWRC, a comparison with the tested and fitted SWRCs for four types of high plasticity clays (without loss of generality) in literature is conducted. All the soils cited here are in relation to the buffer material used in geological nuclear waste repositories, where the nonisothermal condition is particularly prominent. Among them, Boom clay is a natural potential host clay for a repository, while the FEBEX, MX80, and GMZ01 are three types of commonly used sodium bentonites compacted into buffers. All the SWRC datasets are cited or calculated by the raw measurements of suction vs. gravimetric water content in the reference. Besides, the dry density of the specimen for different clays varies from 1.4 to 1.7 Mg/m^3, covering commonly used ranges in the buffers for nuclear waste repositories. The fundamental physical properties of the four high plasticity clays considered in the validation are listed in Table 1, which include parameters given in the literature [69, 89, 92, 98] or back-calculated in this work.

The nonisothermal SWRC model fitted to the data for Boom clay at room temperature and predicted for elevated temperatures are presented in Fig. 9a. The fitting for room temperature data was performed using least-square regression, and the coefficient of determination (R^2) used for evaluating the quality of fit and the root mean square error (*RMSE*) used for evaluation of the difference between the measured data and predicted values are listed in Tables 2 and 4 (see Appendix). The temperatures shown in Fig. 9 and Tables 2 and 4 are shown in °C to be consistent with the literature, but are converted to K for use in the SWRC model. The new SWRC model shows a good fit to the room temperature data with R^2 greater than 0.99 and good prediction with *RMSE* less than 0.03. Similar comparisons of fitted SWRCs for room temperature and predicted SWRCs for elevated temperature with experimental data for FEBEX, MX80 and GMZ01 bentonites are shown in Figs. 9b, c and d, respectively. Although the temperature-dependency of the SWRC may not appear significant in these figures due to the logarithmic scale for suction, the temperature can still have a significant effect that should be considered in coupled heat transfer and water flow analyses. Note that bentonite typically contains large amounts of montmorillonite, which has a higher *CEC* and *SSA* than other constitutent minerals (e.g., kaolinite, illite, quartz, etc.). The variation in suction with saturation changes for bentonites is higher, with a much higher air entry value (lower α) than Boom clay and other clayey, silty, and sandy soils. Thus, compared with Fig. 9a, a flatter evolution in Figs. 9b, c and d is witnessed for the curves under the high suction range, especially in the adsorption. The fitting of room temperature and prediction of elevated temperature curves in Figs. 9b, c and d demonstrated that the proposed SWRC model agrees well with the experimental SWRC data of different bentonites with different dry densities under various temperatures, with R^2 greater than 0.92 and *RMSE* less than 0.06. The difference between SWRCs at different temperatures in Fig. 9 is noticeable. To quantitatively evaluate the temperature effects, the fitting

Table 1 Physical properties of high plasticity clays considered in the validation

No	Soil	G_s (-)	ω_p (%)	ω_0 (g/g)	ρ_d (Mg/m^3)	e (m^3/m^3)	n (m^3/m^3)
1	Boom clay [68, 69]	2.70	29	0.150	1.4	0.934	0.483
2	FEBEX bentonite [92]	2.70	53	0.137	1.5	0.795	0.443
3	MX80 bentonite [89]	2.82	70	0.160	1.6	0.763	0.432
4	GMZ01 bentonite [98]	2.66	37	0.107	1.7	0.565	0.359

Romero et al. [68, 69]; Villar [89]; Villar and Gómez-Espina [92] Wan et al. [98]

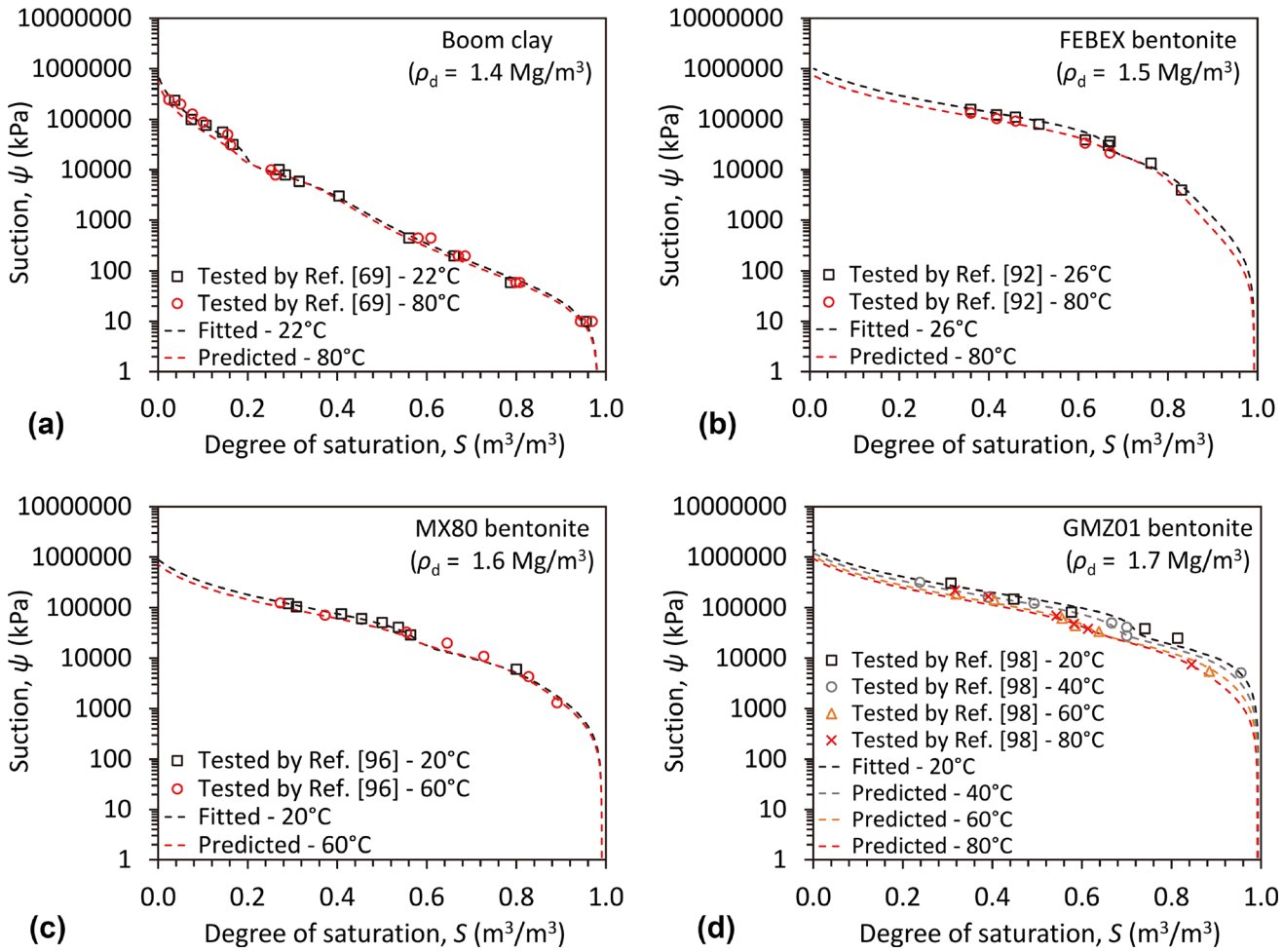

Fig. 9 SWRC calibration for high plasticity clays: **a** Boom clay; **b** Compacted FEBEX bentonite; **c** Compacted MX80 bentonite; **d** Compacted GMZ01 bentonite

Table 2 Nonisothermal SWRC model parameters for the high plasticity clays tested under different temperatures

Soil	T (°C)	Adsorption			Capillarity				Fitting/prediction evaluation	
		ψ_{max} (kPa)	$\theta_{a,max}$ (m^3/m^3)	M (-)	ψ_c (kPa)	α (1/kPa)	χ (K)	N (-)	R^2 (-)	$RMSE$ (-)
Boom clay	22	727,115	0.101	0.085	7129	0.0280	340.3	1.29	0.997	0.015
	80	543,176	0.098		7932	0.0300	317.8		0.994	0.029
FEBEX bentonite	26	1,105,454	0.297	0.132	13,615	0.0033	338.6	1.22	0.983	0.020
	80	802,719	0.295		14,898	0.0055	317.8		0.962	0.021
MX80 bentonite	20	993,009	0.266	0.105	10,213	0.0003	341.2	1.15	0.992	0.015
	60	778,616	0.267		10,857	0.0005	325.0		0.979	0.034
GMZ01 bentonite	20	1,399,239	0.260	0.135	16,250	0.00012	341.2	1.30	0.924	0.048
	40	1,200,343	0.247		16,853	0.00020	332.7		0.993	0.016
	60	1,052,883	0.228		17,424	0.00029	325.0		0.987	0.022
	80	940,545	0.228		17,961	0.00050	317.8		0.932	0.054

Table 3 Quantitative comparison of relative differences between degrees of saturation at highest and lowest temperatures in Fig. 9

Soil	T	ψ = 113,000 kPa		ψ = 38,000 kPa		ψ = 4200 kPa	
	(°C)	S (m^3/m^3)	δ (%)	S (m^3/m^3)	δ (%)	S (m^3/m^3)	δ (%)
Boom clay	22	0.080	28.20	0.167	16.96	0.388	2.200
	80	0.058		0.139		0.380	
FEBEX bentonite	26	0.460	19.85	0.654	5.211	0.838	2.365
	80	0.369		0.620		0.818	
MX80 bentonite	20	0.305	16.84	0.533	6.069	0.821	0.806
	60	0.254		0.501		0.814	
GMZ01 bentonite	20	0.494	30.46	0.641	16.10	0.927	11.95
	80	0.343		0.538		0.816	

values and the relative error between the highest (80 °C) and lowest (~ 22 °C) temperature for three specific suctions (113000, 38000, and 4200 kPa) which are commonly selected by vapor equilibrium technique in literature [54, 96, 99] are listed in Table 3. The relative error is defined as follows:

$$\delta = \frac{S_{T_2} - S_{T_1}}{S_{T_1}} \tag{30}$$

where δ is the relative error, T_1 and T_2 are the lowest and highest temperature, respectively, and S_T is the degree of saturation at temperature T. Although the values of ψ_{max} in Table 2 were treated as a fitting parameter for these soils as it is difficult to determine experimentally, the values show good agreement with previous modeling works and assumptions [46, 119].

A comparison between the fitted *CEC* and *SSA* at the reference temperature and values measured in the literature [30, 40, 81, 89, 90, 93, 98, 104, 106, 111, 121] is shown in Figs. 10a and b, respectively. Results in Fig. 10a demonstrated that the fitted *CEC* is consistent with the tested data, as the fitted and tested values follow the 1: 1 line with R^2 of 0.97. Meanwhile, although the fitted and tested *SSA* values are correlated R^2 of 0.76, it is interesting to note that the fitted *SSA* is overpredicted, meaning that the fitted *SSA* is usually greater than the measured *SSA* (Fig. 10b). In fact, the *SSA* value used in this study is for predicting the ψ_c (Eq. (25)), which controls the SWRC shap at the transition between the adsorption and capillarity water retention mechanisms. If a lower value of *SSA* is used, a stepped curve is observed. Thus, for smooth and coherent SWRC, a higher value of *SSA* than measured in the literature is adopted here. Besides, the *SSA* measurement is method dependent, and the measured value might vary with batches of samples.

Experimental tests have highlighted the variability in pore size within clayey soil, with pores smaller than a certain threshold believed to be difficult to further compress [44]. Such micro pores are commonly assumed to be saturated in order to simplify modeling efforts [21], despite the fact that the pore size distribution can be influenced by various factors including mineral composition, saturation level, among others. Although various methods exist for differentiating between micro and macro pores, a threshold value of pore size in the pore size distribution functions is commonly used [45, 77]. Specifically, a threshold of 150 nm is widely applied for high plasticity clay [44, 105]. Using the same threshold value on the mercury intrusion porosimetry (MIP) data of the four high plasticity clays [28, 45, 69, 94], the relationship between the "ratio of micropores to total pores (e_m/e)" and the "ratio of adsorption capacity to saturated water content ($\theta_{a,max}/\theta_s$)", is depicted in Fig. 11. The MIP tests were conducted on the four clays with similar densities (1.4–1.7 Mg/m^3) under similar suction ranges (4–43 MPa). The results in Fig. 11 show a strong linear correlation between the two parameters, indicating the feasibility of estimating the adsorption capacity $\theta_{a,max}$ from pore size data.

Another evaluation of the new SWRC can be conducted regarding the temperature dependency of the model parameter α in Eq. (29). Note that the value of α adapted for fitting SWRCs increases with increasing temperature (Table 2), as α is typically assumed equal to the inverse of air entry suction (Eq. (26)). A summary of the calculated air entry suction ($\psi_{aev} = 1/\alpha$) for the four clays is shown in Fig. 12. Results in the figure show that the air entry suction decreases with increasing temperature, while the decreasing rate is soil-texture dependence. The fitted air entry suction for GMZ01 bentonite is consistent with the value measured in the literature [99]. Generally, a decrease in the air entry suction with increasing dry density is observed.

5 Conclusions

This paper presents a general soil water retention curve that accounts for the effects of temperature on both adsorption and capillarity water retention mechanisms in unsaturated soils under confined conditions. For the adsorption water retention mechanism, a negative correlation between

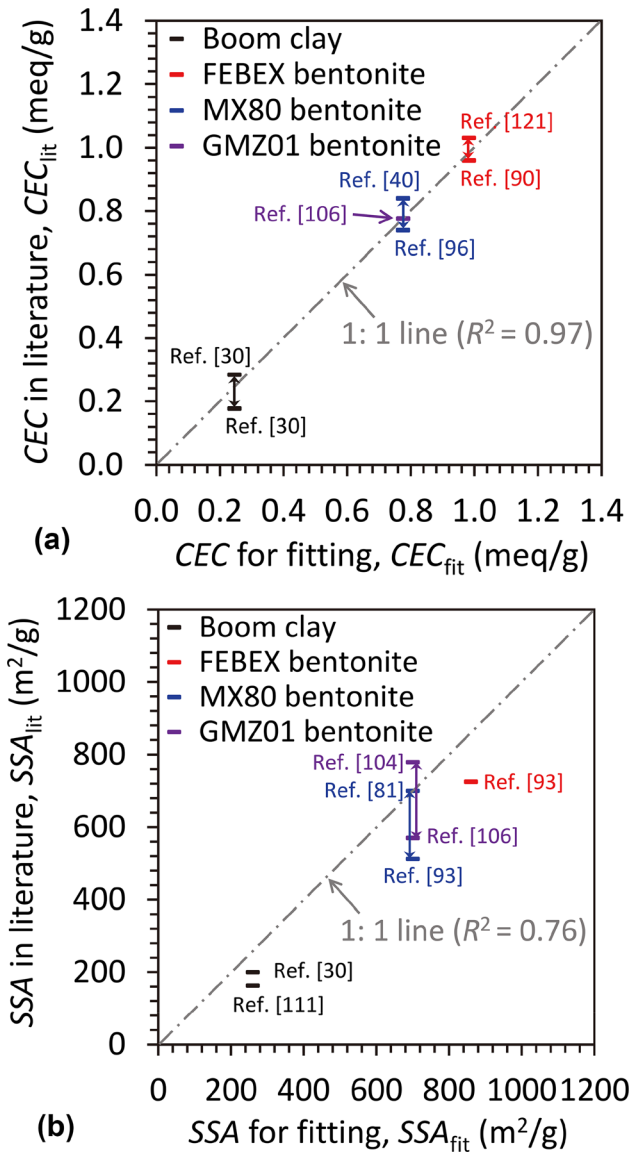

Fig. 10 Comparison of *CEC* and *SSA* from fitting analysis and measured in literature. Honty [30]; Kumpulainen and Kiviranta[40]; Tessier et al. [81]; Villar et al. [90]; Villar et al. [93]; Villar [96]; Wu et al. [104]; Ye et al. [106]; Yukselen and Kaya [111]; Červinka and Kolomá [121]

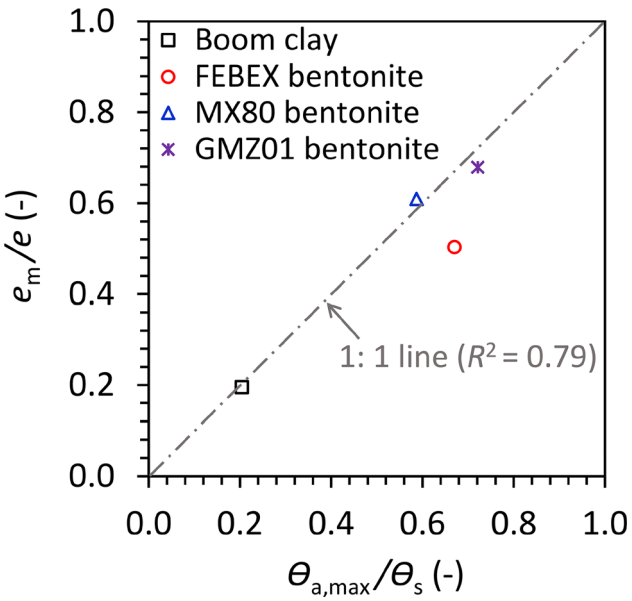

Fig. 11 Relationship between micropore content and adsorption capacity

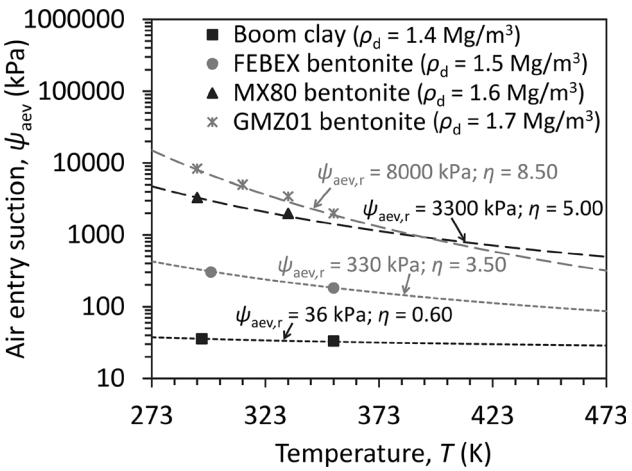

Fig. 12 Summary of the temperature dependence of the air entry suction (inverse of α)

maximum matric suction and temperature was analyzed through BET theory. Additionally, a new non-monotonic *CEC*-temperature equation was proposed for characterizing the temperature effect on adsorption capacity. For the capillarity water retention mechanism, the mean cavitation suction, related to the transition between capillarity to adsorption water retention mechanisms, was studied along with the widely known temperature-sensitive parameters such as surface tension, contact angle, and air entry suction. A relationship between the mean cavitation suction and basic soil physical parameters such as the *SSA* and dry density was developed. The mean cavitation suction, which pertains to the curve continuity around the physical-phase transition point between the adsorption and capillarity water retention mechanisms, shows a positive correlation with elevated temperature. The proposed nonisothermal SWRC model was validated using data from the literature for high plasticity clays having different dry densities, including natural clay and compacted bentonites. Model predictions with high R^2 indicate that the proposed model can simulate the tested data well under different temperatures by considering temperature effects on adsorption and capillarity water retention mechanisms. The new nonisothermal SWRC model will be useful for simulating coupled heat transfer and water flow processes in hydrogeologic and geotechnical applications involving elevated temperatures.

Appendix

Table 4 Supplementary model parameters for Table 2

Soil	T (°C)	Adsorption			Capillarity		
		c (-)	CEC (meq/g)	b_w (g/g)	A_H (kPa)	ΔH (J/m^2)	SSA (m^2/g)
Boom Clay	22	16.00	0.246	0.11	7,129	− 0.515	260
	80	9.99	0.249	0.10	7,932	− 0.481	
FEBEX bentonite	26	24.00	0.983	0.18	13,615	− 0.512	860
	80	14.76	0.993	0.16	14,898	− 0.481	
MX80 bentonite	20	22.00	0.776	0.18	10,213	− 0.516	700
	60	15.18	0.789	0.17	10,857	− 0.491	
GMZ01 bentonite	20	31.00	0.776	0.25	16,250	− 0.516	700
	40	24.90	0.778	0.23	16,853	− 0.503	
	60	20.53	0.784	0.20	17,424	− 0.491	
	80	17.30	0.787	0.20	17,961	− 0.481	

The parameters listed here are used to calculate the parameters in Table 2

Acknowledgements The authors appreciate support from US Department of Energy Nuclear Energy University Program award DE-NE008951. The views in this paper are those of the authors alone.

Data availability All data generated or analyzed during this study are included in this published article.

References

1. Akinwunmi B, Sun L, Hirvi JT, Kasa S, Pakkanen TA (2019) Influence of temperature on the swelling pressure of bentonite clay. Chem Phys 516:177–181
2. Alsherif NA, McCartney JS (2015) Thermal behaviour of unsaturated silt at high suction magnitudes. Géotechnique 65(9):703–716
3. Alsherif N, Wayllace A, Lu N (2015) Measuring the soil water–retention curve under positive and negative matric suction regimes. Geotech Test J 38(4):442–451
4. Bachmann J, Horton R, Grant SA, Van der Ploeg RR (2002) Temperature dependence of water retention curves for wettable and water-repellent soils. Soil Sci Soc Am J 66(1):44–52
5. Bag R, Rabbani A (2017) Effect of temperature on swelling pressure and compressibility characteristics of soil. Appl Clay Sci 136:1–7
6. Behbehani F, McCartney JS (2022) Energy pile groups for thermal energy storage in unsaturated soils. Appl Therm Eng 215:119028
7. Brennen CE (2014) Cavitation and bubble dynamics. Cambridge University Press
8. Brooks RH, Corey AT (1964) Hydraulic properties of porous media. Hydrology Paper No 3. Civil Engineering Department, Colorado State University, Fort Collins, CO
9. Brunauer S, Emmett PH, Teller E (1938) Adsorption of gases in multimolecular layers. J Am Chem Soc 60(2):309–319
10. Cheng Q, Zhou C, Ng CWW, Tang C (2020) Thermal effects on water retention behaviour of unsaturated collapsible loess. J Soils Sediments 20:756–762
11. De la Morena G, Navarro V, Asensio L, Gallipoli D (2021) A water retention model accounting for void ratio changes in double porosity clays. Acta Geotech 16:2775–2790
12. Dong Y, McCartney JS, Lu N (2015) Critical review of thermal conductivity models for unsaturated soils. Geotech Geol Eng 33:207–221
13. Fernández DP, Goodwin ARH, Lemmon EW, Levelt Sengers JMH, Williams RC (1997) A formulation for the static permittivity of water and steam at temperatures from 238 K to 873 K at pressures up to 1200 MPa, including derivatives and Debye-Hückel coefficients. J Phys Chem Ref Data 26(4):1125–1166
14. Ferrari A, Bosch JA, Baryla P, Rosone M (2022) Volume change response and fabric evolution of granular MX80 bentonite along different hydro-mechanical stress paths. Acta Geotech 17(9):3719–3730
15. François B, Ettahiri S (2012) Role of the soil mineralogy on the temperature dependence of the water retention curve. In: Unsaturated soils: research and application. 2nd European conference on unsaturated soils (E-UNSAT 2012), Napoli, Italy
16. Fredlund DG (2019) State of practice for use of the soil-water characteristic curve (SWCC) in geotechnical engineering. Can Geotech J 56(8):1059–1069

17. Fredlund DG, Xing A (1994) Equations for the soil-water characteristic curve. Can Geotech J 31(4):521–532
18. Fredlund DG, Xing A, Fredlund MD, Barbour SL (1996) The relationship of the unsaturated soil shear strength to the soil-water characteristic curve. Can Geotech J 33(3):440–448
19. Gao Y, Sun DA, Zhu ZC, Xu YF (2019) Hydromechanical behavior of unsaturated soil with different initial densities over a wide suction range. Acta Geotech 14:417–428
20. Gee GW, Campbell MD, Campbell GS, Campbell JH (1992) Rapid measurement of low soil water potentials using a water activity meter. Soil Sci Soc Am J 56(4):1068–1070
21. Gens A, Alonso EE (1992) A framework for the behaviour of unsaturated expansive clays. Can Geotech J 29(6):1013–1032
22. Ghavam-Nasiri A, El-Zein A, Airey D, Rowe RK (2019) Water retention of geosynthetics clay liners: dependence on void ratio and temperature. Geotext Geomembr 47(2):255–268
23. Go S, Lyapustin A, Schuster GL, Choi M, Ginoux P, Chin M, Kalashnikova O, Dubovik O, Kim J, da Silva A, Holben B, Reid JS (2022) Inferring iron-oxide species content in atmospheric mineral dust from DSCOVR EPIC observations. Atmos Chem Phys 22(2):1395–1423
24. Goodman CC, Latifi N, Vahedifard F (2018) Effects of temperature on microstructural properties of unsaturated clay. In IFCEE 2018:343–352
25. Grant SA, Salehzadeh A (1996) Calculation of temperature effects on wetting coefficients of porous solids and their capillary pressure functions. Water Resour Res 32(2):261–270
26. Grimsel Test Site (GTS) (2022) HotBENT Introduction. http://web.archive.org/web/20220525182521/https://grimsel.com/gts-projects/hotbent-high-temperature-effects-on-bentonite-buffers/hotbent-introduction, Accessed on 07/22/2023
27. Haar L, Gallagher JS, Kell GS (1984) NBS/NRC steam table. Hemisphere Publishing Corporation, New York
28. He Y (2017) Volume change behavior of highly compacted GMZ bentonite under chemo-hydro-mechanical conditions. Ph.D. dissertation, Tongji University, Shanghai
29. Herbert E, Balibar S, Caupin F (2006) Cavitation pressure in water. Phys Rev E 74(4):041603
30. Honty M (2010) CEC of the Boom Clay – a review. External Report of the Belgian Nuclear Research Centre, Mol, Belgium, SCK· CENÀERÀ134
31. Israelachvili JN (1991) Aggregation of amphiphillic molecules into micelles, bilayers, vesicles and biological membranes. Academic Press, San Diego, Intermolecular and Surface Forces
32. Iwamatsu M, Horii K (1996) Capillary condensation and adhesion of two wetter surfaces. J Colloid Interface Sci 182(2):400–406
33. Jacinto AC, Villar MV, Gómez-Espina R, Ledesma A (2009) Adaptation of the van Genuchten expression to the effects of temperature and density for compacted bentonites. Appl Clay Sci 42(3–4):575–582
34. Kendir E, Yaltkaya Ş (2022) Effect of temperature and wavelength on the refractive index of water: a fiber-optic sensor application. Ind J Phys 96:1247–1252
35. Khalili NGFA, Geiser F, Blight GE (2004) Effective stress in unsaturated soils: Review with new evidence. Int J Geomech 4(2):115–126
36. Khorshidi M, Lu N (2017) Intrinsic relation between soil water retention and cation exchange capacity. J Geotech Geoenviron Eng 143(4):04016119
37. Khorshidi M, Lu N (2017) Quantification of exchangeable cations using soil water retention curve. J Geotech Geoenviron Eng 143(9):04017057
38. Khorshidi M, Lu N, Akin ID, Likos WJ (2017) Intrinsic relationship between specific surface area and soil water retention. J Geotech Geoenviron Eng 143(1):04016078
39. Kocaman K, Ozocak A, Edil TB, Bol E, Sert S, Onturk K, Ozsagir M (2022) Evaluation of soil-water characteristic curve and pore-size distribution of fine-grained soils. Water 14(21):3445
40. Kumpulainen S, Kiviranta L (2010). Mineralogical and chemical characterization of various bentonite and smectite-rich clay materials Part A: Comparison and development of mineralogical characterization methods Part B: Mineralogical and chemical characterization of clay materials (No. POSIVA-WR–10–52). Posiva Oy
41. Leung AK, Feng S, Vitali D, Ma L, Karimzadeh AA (2020) Temperature effects on the hydraulic properties of unsaturated sand and their influences on water-vapor heat transport. J Geotech Geoenviron Eng 146(4):06020003
42. Lifshitz EM (1955) The theory of molecular attraction forces between solid bodies. Zhurnal Eksperimentalnoi Teoreticheskoi Fiziki 29:94–110
43. Liu ZR, Ye WM, Cui YJ, Zhu HH, Wang Q, Chen YG (2021) Insights into the water retention behaviour of GMZ bentonite pellet mixture. Acta Geotech 16(10):3145–3160
44. Lloret A, Villar MV (2007) Advances on the knowledge of the thermo-hydro-mechanical behaviour of heavily compacted "FEBEX" bentonite. Phys Chem Earth Parts A/B/C 32(8–14):701–715
45. Lloret A, Villar MV, Sanchez M, Gens A, Pintado X, Alonso EE (2003) Mechanical behaviour of heavily compacted bentonite under high suction changes. Géotechnique 53(1):27–40
46. Lu N (2016) Generalized soil water retention equation for adsorption and capillarity. J Geotech Geoenviron Eng 142(10):04016051
47. Lu N, Godt JW, Wu DT (2010) A closed-form equation for effective stress in unsaturated soil. Water Resour Res 46(5):W05515
48. Lu N, Kaya M (2013) A drying cake method for measuring suction-stress characteristic curve, soil-water-retention curve, and hydraulic conductivity function. Geotech Test J 36(1):1–19
49. Lu N, Khorshidi M (2015) Mechanisms for soil-water retention and hysteresis at high suction range. J Geotech Geoenviron Eng 141(8):04015032
50. Lu N, Zhang C (2019) Soil sorptive potential: Concept, theory, and verification. J Geotech Geoenviron Eng 145(4):04019006
51. Lu Y, McCartney JS (2022) Physical modeling of coupled thermohydraulic behavior of compacted MX80 bentonite during heating. Geotech Test J 45(6):20220054
52. Lu Y, McCartney JS (2024) Insights into the thermo-hydraulic properties of compacted MX80 bentonite during hydration under elevated temperature. Can Geotech J 61:344–360
53. Lu Y, McCartney JS (2024) Thermal conductivity function for fine-grained unsaturated soils linked with water retention by capillarity and adsorption. J Geotech Geoenviron Eng 150(1):06023009
54. Lu Y, Ye WM, Wang Q, Chen YG (2023) Insights into anisotropic swelling pressure of compacted GMZ bentonite. Acta Geotech 18:5721–5734
55. Lu Y, Ye WM, Wang Q, Zhu YH, Chen YG, Chen B (2020) Investigation on anisotropic thermal conductivity of compacted GMZ bentonite. Bull Eng Geol Environ 79:1153–1162
56. Lu Y, Ye WM, Wang Q, Zhu YH, Chen YG, Chen B (2021) Anisotropic swelling behaviour of unsaturated compacted GMZ bentonite hydrated under vertical stresses. Bull Eng Geol Environ 80(7):5515–5526
57. Lu Y, Zapata CE (2016) Temperature effects on the unsaturated hydraulic properties of two fine-grained soils and their influence on moisture movement under an airfield test facility. Geotech Struct Eng Congress 2016:569–583

58. Luo S, Likos WJ, Lu N (2021) Cavitation of water in soil. J Geotech Geoenviron Eng 147(8):04021079
59. Marshall WL (2008) Dielectric constant of water discovered to be simple function of density over extreme ranges from –35 to +600°C and to 1200 MPa (12000 Atm) Believed Universal. Nat Precedings. https://doi.org/10.1038/npre.2008.2472.1
60. McCartney JS (2022) Water retention in expansive clay under elevated temperatures and constrained conditions. In Geo-Congress 2022:315–324
61. McQueen IS, Miller RF (1974) Approximating soil moisture characteristics from limited data: Empirical evidence and tentative model. Water Resour Res 10(3):521–527
62. Mitchell JK, Soga K (2005) Fundamentals of soil behavior, 3rd edn. Wiley, New York
63. Pham TA, Hashemi A, Sutman M, Medero GM (2023) Effect of temperature on the soil–water retention characteristics in unsaturated soils: Analytical and experimental approaches. Soils Found 63(3):101301
64. Pusch R (1992) Use of bentonite for isolation of radioactive waste products. Clay Miner 27(3):353–361
65. Qian JG, Lin ZQ, Shi ZH (2022) Experimental and modeling study of water-retention behavior of fine-grained soils with dual-porosity structures. Acta Geotech 17(8):3245–3258
66. Revil A, Lu N (2013) Unified water isotherms for clayey porous materials. Water Resour Res 49(9):5685–5699
67. Rojas E, Chávez O, Arroyo H, López-Lara T, Hernández JB, Horta J (2017) Modeling the dependency of soil-water retention curve on volumetric deformation. Int J Geomech 17(1):04016039
68. Romero E, Gens A, Lloret A (2001) Temperature effects on the hydraulic behaviour of an unsaturated clay. Unsaturated Soil Concepts and Their Application in Geotechnical Practice, Dordrecht, Springer, pp 311–332
69. Romero E, Gens A, Lloret A (2003) Suction effects on a compacted clay under non-isothermal conditions. Géotechnique 53(1):65–81
70. Roshani P, Sedano JÁI (2016) Incorporating temperature effects in soil-water characteristic curves. Ind Geotech J 46:309–318
71. Ruan K, Komine H, Ito D, Miyoshi K, Gotoh T (2022) Hydraulic conductivity and X-ray diffraction tests of unsaturated bentonites with a multi-ring and their predictions by pores distributions. Eng Geol 306:106738
72. Salager S, Rizzi M, Laloui L (2011) An innovative device for determining the soil water retention curve under high suction at different temperatures. Acta Geotech 6:135–142
73. Sanchez M (2004) Thermo-hydro-mechanical coupled analysis in low permeability media, Doctoral dissertation, Universitat Politècnica de Catalunya (UPC)
74. Sarikaya Y, Önal M, Baran B, Alemdaroğlu T (2000) The effect of thermal treatment on some of the physicochemical properties of a bentonite. Clays Clay Miner 48(5):557–562
75. Schiebener P, Straub J, Levelt Sengers JMH, Gallagher JS (1990) Refractive index of water and steam as function of wavelength, temperature and density. J Phys Chem Ref Data 19(3):677–717
76. Schneider M, Goss KU (2011) Temperature dependence of the water retention curve for dry soils. Water Resour Res 47(3):W03506
77. Seiphoori A, Ferrari A, Laloui L (2014) Water retention behaviour and microstructural evolution of MX-80 bentonite during wetting and drying cycles. Géotechnique 64(9):721–734
78. She HY, Sleep BE (1998) The effect of temperature on capillary pressure-saturation relationships for air-water and perchloroethylene-water systems. Water Resour Res 34(10):2587–2597
79. Spagnoli G, Stanjek H, Sridharan A (2012) Influence of ethanol/water mixture on the undrained shear strength of pure clays. B Eng Geol Environ 71:389–398
80. Tang AM, Cui YJ (2005) Controlling suction by the vapour equilibrium technique at different temperatures and its application in determining the water retention properties of MX80 clay. Can Geotech J 42(1):287–296
81. Tessier D, Dardaine M, Beaumont A, Jaunet AM (1998) Swelling pressure and microstructure of an activated swelling clay with temperature. Clay Miner 33(2):255–267
82. Thomas PJ, Baker JC, Zelazny LW (2000) An expansive soil index for predicting shrink–swell potential. Soil Sci Soc Am J 64(1):268–274
83. Tuller M, Or D (2005) Water films and scaling of soil characteristic curves at low water contents. Water Resour Res 41(9):W09403
84. Thyagaraj T, Rao SM (2010) Influence of osmotic suction on the soil-water characteristic curves of compacted expansive clay. J Geotech Geoenviron Eng 136(12):1695–1702
85. Thyagaraj T, Thomas SR, Das AP (2017) Physico-chemical effects on shrinkage behavior of compacted expansive clay. Int J Geomech 17(2):06016013
86. Uchaipichat A, Khalili N (2009) Experimental investigation of thermo-hydro-mechanical behaviour of an unsaturated silt. Géotechnique 59(4):339–353
87. Vahedifard F, Cao TD, Thota SK, Ghazanfari E (2018) Non-isothermal models for soil–water retention curve. J Geotech Geoenviron Eng 144(9):04018061
88. van Genuchten MT (1980) A closed-form equation for predicting the hydraulic conductivity of unsaturated soils. Soil Sci Soc Am J 44(5):892–898
89. Villar MV (2005) MX-80 Bentonite. Thermo-Hydro-Mechanical Characterisation Performed ad CIEMAT in the Context of the Prototype Project. Informes Técnicos Ciemat 1053, Departamento de Impacto Ambiental de la Energía, Spain
90. Villar MV, Fernández AM, Romero E, Dueck A, Cuevas J, Plötze M, Kaufhold S, Dohrmann R, Iglesias RJ, Sakaki T, Voltolini M, Zheng L, Kawamoto K. Kober F (2017) FEBEX-DP Post-mortem THM/THG Analysis Report. Nagra Arbeitsbericht, NAB 16–17, Nagra, Wettingen, Switzerland, 187 pp
91. Villar MV, Gómez-Espina R (2007) Retention curves of two bentonites at high temperature. Experimental unsaturated soil mechanics. Springer, Berlin Heidelberg, pp 267–274
92. Villar MV, Gómez-Espina R (2008) Effect of temperature on the water retention capacity of FEBEX and MX-80 bentonites. Unsaturated Soils. CRC Press, Advances in Geo-Engineering, pp 273–278
93. Villar MV, Gómez-Espina R, Lloret A (2010) Experimental investigation into temperature effect on hydro-mechanical behaviours of bentonite. J Rock Mech Geotech Eng 2(1):71–78
94. Villar MV, Gomez-Espina R, Campos R, Gutierrez-Nebot L, Barrios I (2014) Retention curves of bentonite under a microstructural perspective. Research & Applications. CRC Press, In Unsaturated Soils, pp 989–994
95. Villar MV, Lloret A (2004) Influence of temperature on the hydro-mechanical behaviour of a compacted bentonite. Appl Clay Sci 26(1–4):337–350
96. Villar MV, Martín PL, Lloret A (2005) Retention curves of two bentonites at high tenperature. Exper Unsaturated Soil Mech EXPERUS 2005:267–274
97. Wada K, Harada Y (1971) Effects of temperature on the measured cation-exchange capacities of Ando soils. J Soil Sci 22(1):109–117
98. Wan M (2010) Study on soil-water characteristics and permeability of highly compacted GMZ bentonite with temperature control. Ph.D. dissertation, Tongji University, Shanghai

99. Wan M, Ye WM, Chen YG, Cui YJ, Wang J (2015) Influence of temperature on the water retention properties of compacted GMZ01 bentonite. Environ Earth Sci 73:4053–4061
100. Wang H, Chen R, Leung AK, Huang J (2023) Temperature effects on the hydraulic properties of unsaturated rooted soils. Can Geotech J 60(6):936–945
101. Watson KM (1943) Thermodynamics of the liquid state. Ind Eng Chem Res 35(4):398–406
102. Weast RC, Astle MJ, Beyer WH (1985) CRC Handbook of Chemistry and Physics, pp. F174–F184
103. White I, Zegelin SJ, Topp GC, Fish A (1994) Effect of bulk electrical conductivity on TDR measurement of water content in porous media. In: Proceedings of a symposium and workshop on time domain reflectometry in environmental, infrastructure and mining applications, September 7–9, 1994, Evanston, IL
104. Wu T, Yang Y, Wang Z, Shen Q, Tong Y, Wang M (2020) Anion diffusion in compacted clays by pore-scale simulation and experiments. Water Resour Res 56(11):e2019WR027037
105. Xu Y, Sun DA, Zeng Z, Lv H (2019) Effect of aging on thermal conductivity of compacted bentonites. Eng Geol 253:55–63
106. Ye WM, Cui YJ, Qian LX, Chen B (2009) An experimental study of the water transfer through confined compacted GMZ bentonite. Eng Geol 108(3–4):169–176
107. Ye WM, Lu Y, Huang XH, Chen B, Chen YG, Cui YJ (2017) Anisotropic thermal conductivity of unsaturated compacted GMZ bentonite-sand mixture. In PanAm Unsaturated Soils 2017:413–424
108. Ye WM, Wan M, Chen B, Chen YG, Cui YJ, Wang J (2013) Temperature effects on the swelling pressure and saturated hydraulic conductivity of the compacted GMZ01 bentonite. Environ Earth Sci 68:281–288
109. Yilmaz I (2006) Indirect estimation of the swelling percent and a new classification of soils depending on liquid limit and cation exchange capacity. Eng Geol 85(3–4):295–301
110. Young T (1805) III. An essay on the cohesion of fluids. Philos Trans R Soc Lond B Biol Sci 95:65–87
111. Yukselen Y, Kaya A (2008) Suitability of the methylene blue test for surface area, cation exchange capacity and swell potential determination of clayey soils. Eng Geol 102:38–45
112. Zhai Q, Zhu YY, Rahardjo H, Satyanaga A, Dai GL, Gong WM, Zhao XL, Ou YZ (2023) Prediction of the soil–water characteristic curves for the fine-grained soils with different initial void ratios. Acta Geotech 18:5359–5368
113. Zhang C, Hu S, Qiu Z, Lu N (2022) A poroelasticity theory for soil incorporating adsorption and capillarity. Géotechnique. https://doi.org/10.1680/jgeot.22.00097
114. Zhang C, Lu N (2020) Unified effective stress equation for soil. J Eng Mech 146(2):04019135
115. Zhang JR, Niu G, Li XC, Sun DA (2020) Hydro-mechanical behavior of expansive soils with different dry densities over a wide suction range. Acta Geotech 15:265–278
116. Zhang Z, Cui YJ, Yang JW, Mokni N, Ye WM, He Y (2022) Water retention and compression behavior of MX80 bentonite pellet. Acta Geotech 17(6):2435–2447
117. Zheng LG, Rutqvist J, Birkholzer JT, Liu HH (2015) On the impact of temperatures up to 200 °C in clay repositories with bentonite engineer barrier systems: a study with coupled thermal, hydrological, chemical, and mechanical modeling. Eng Geol 197:278–295
118. Zhou AN, Sheng DC, Li J (2014) Modelling water retention and volume change behaviours of unsaturated soils in non-isothermal conditions. Comput Geotech 55:1–13
119. Zhu YH, Ye WM, Wang Q, Lu Y, Chen YG (2020) Anisotropic volume change behaviour of uniaxial compacted GMZ bentonite under free swelling condition. Eng Geol 278:105821
120. Önal M (2007) Swelling and cation exchange capacity relationship for the samples obtained from a bentonite by acid activations and heat treatments. Appl Clay Sci 37(1–2):74–80
121. Červinka R, Kolomá K (2016) Determination of CEC and exchangeable cations on sample BS-36–3. Technical report 39/2016/ENG, ÚJV Řež, a. s., Prague